Manuscript for Biogeosciences

Title: Evaluation of modeled global carbon dynamics: analysis based on global carbon flux and above-ground biomass data

Running Title: Evaluation of modeled global carbon dynamics

Bao-Lin Xue[1], Qinghua Guo[1, 2,*], Tianyu Hu[1], Yongcai Wang[1], Shengli Tao[1], Yanjun Su[2], Jin Liu[1] and Xiaoqian Zhao[1]

[1]State Key Laboratory of Vegetation and Environmental Change, Institute of Botany, Chinese Academy of Sciences, No. 20 Nanxincun, Xiangshan, Beijing 100093, China

[2]School of Engineering, Sierra Nevada Research Institute, University of California at Merced, CA 95343, USA

Author Agreement:

All authors agree on the authorship of the manuscript and approve the submission.

***Corresponding author:**

Qinghua Guo, Dr., Prof.

State Key Laboratory of Vegetation and Environmental Change, Institute of Botany, Chinese Academy of Sciences, No. 20 Nanxincun, Xiangshan, Beijing 100093, China

Tel.: +86-10-6283-6473

Email: guo.qinghua@gmail.com

Abstract

Dynamic global vegetation models are useful tools for the simulation of global carbon cycle. However, most models are hampered by the poor availability of global aboveground biomass (AGB) data, which is necessary for the model calibration process. Here, taking the integrated biosphere simulator model (IBIS) as an example, we evaluated the modeled carbon dynamics, including gross primary production (GPP) and potential AGB, at the global scale. The IBIS model was constrained by both in situ GPP and plot-level AGB data collected from the literature. Model results showed that IBIS could reproduce GPP with acceptable accuracy in monthly and annual scales. At the global scale, the IBIS-simulated total AGB was similar to those obtained in other studies. However, discrepancies were observed between the model-derived and observed AGB for pan-tropical forests. The bias in modeled AGB was mainly caused by the single-parameter set of the model. This study also showed that different meteorological inputs can introduce substantial differences in modeled AGB in the global scale, although this difference is small compared with parameter-induced differences. The conclusions of our research highlight the necessity of considering the heterogeneity of key model physiological parameters in modeling global AGB. The main conclusions of our research will help to improve model simulated global carbon cycles.

Keywords: dynamic global vegetation model, integrated biosphere model, gross primary production, above-ground biomass, global carbon cycle

1 Introduction

The global terrestrial ecosystem is an important carbon sink that can mitigate the ongoing increases in atmospheric CO_2 concentration (Dixon et al., 1994; Luyssaert et al., 2007; Pan et al., 2011). For example, global forests, which cover around 30% of the land surface, account for ~75% of terrestrial gross primary production (GPP) and ~80% of global plant biomass (Kindermann et al., 2008; Beer et al., 2010). The large carbon stock in the terrestrial ecosystem indicates the need for a reliable description of its current distribution (Keith et al., 2009; Galbraith et al., 2010; Pan et al., 2011; Xue et al., 2011). However, it is still a challenge to accurately estimate the distribution of carbon stocks on the global scale, mainly because of the lack of good observations as well as the unknown mechanisms and/or relative contributions of various factors such as climate change, CO_2 fertilization, and land use change on carbon dynamics (McGuire et al., 2001; Mu et al., 2008).

Various methods have been developed for mapping the global distribution of biomass, and each has its pros and cons. On the regional scale, the field inventory method provides the most reliable information on biomass, but it is labor intensive and costly when applied over a large area (e.g., Malhi et al., 2002). On the global scale, remote-sensing methods have advantages over field inventory methods for applications to large areas and in areas that are difficult to access (Lefsky et al., 2005; Thurner et al., 2014; Tao et al., 2014). For example, the light detection and ranging method has recently been used in the Amazon region, with acceptable accuracy (Asner et al., 2010; Saatchi et al., 2011). As an alternative, the dynamic global vegetation model (DGVM) is a useful tool for mapping global biomass and is the only method that predicts future variations. In the past, many researchers have explored how climate change or land use change would influence the global biomass, and this

has improved our understanding in the projection of terrestrial responses to climate change. In many cases, the DGVM-modeled potential vegetation biomass is used as a baseline for exploring the corresponding response to the projected climate. Before using the DGVM to project future biomass changes, an evaluation of how the DGVM can reproduce potential (natural) present-day biomass is necessary (Mu et al., 2008; Seiler et al., 2014). However, this is rarely done, mainly because of the lack of available global-scale biomass data. For instance, in many cases, the default values for various physiological parameters are used, and may differ greatly for different DGVMs. The lack of evaluation of modeled biomass on the global scale may result in large differences among global carbon stocks obtained using different models (Cramer et al., 2001; Sitch et al., 2008), resulting in bias in our conclusions regarding vegetation responses in projected climate scenarios (Huntingford et al., 2008; 2013).

Uncertainty in the modeled biomass may originate in various ways: model structure, model parameters, and meteorological inputs. The results for potential natural vegetation obtained from bioclimatic limits and forest dynamics using the DGVM may give an unrealistic representation of competition among plant functional types (PFTs) (Purves and Pacala, 2008; Seiler et al., 2014). A biased PFT in the DGVM partly contributes to the uncertainty in carbon dynamics, including GPP and biomass. Moreover, DGVMs usually use a single set of parameters to represent different biomes and rarely consider spatial heterogeneity (Xiao et al., 2011, 2014). In reality, different physiological parameters vary greatly, depending on the soil type, climate, and vegetation (Castanho et al., 2013). The ways in which this will bias the spatial pattern of carbon flux, and thus biomass accumulation, have not been sufficiently discussed on the global scale, partly because of the unavailability of biomass data for large areas (Delbart et al., 2010; Wolf et al., 2011). Recent research

has shown that it is necessary to use both carbon flux data and biometric data for DGVM calibration (Kondo et al., 2013; Seiler et al., 2014). Furthermore, uncertainties in DGVM-derived carbon flux and biomass may also arise from the input data itself, such as meteorological forcing data (Barman et al., 2014a, b). Different input data can result in differences among the results obtained using different models when modeling large-scale carbon flux (Zhao et al., 2005). It is therefore necessary to quantify the uncertainty from meteorological inputs in modeled biomass, to improve the modeling results.

The objective of this study is to evaluate model-derived carbon flux and biomass on the global scale using collected carbon flux (GPP) and biomass datasets at the plot level. To do this, we used the integrated biosphere simulator (IBIS; Foley et al., 1996; Kucharik et al., 2000) as an example, and used both carbon flux and collected above-ground biomass (AGB) data to constrain the model. We adopted the most important parameters from meta-analysis, calibration, or from the literature. We also investigated how different meteorological input data changed the modeling results. Overall, the intention of the current study was to explore the following questions. 1) How accurately can IBIS simulate GPP and AGB, and where does bias originate? 2) Can a single set of calibrated parameters accurately map the patterns of GPP and AGB? 3) What should modelers do to improve the modeling results?

2 Material and methods

2.1 IBIS model

The IBIS model considers the composition and structure of vegetation responses to environmental changes, within an integrated framework, to simulate land surface hydrological processes, biogeochemical cycles, and terrestrial vegetation dynamics. The model simulates the land surface processes for energy, water, and momentum

exchange between soil, vegetation, and the atmosphere, using a land surface transfer scheme (LSX) (Thompson and Pollard, 1995a, b). Two canopy layers, three snow layers, and six soil layers are considered in each grid unit. Evapotranspiration (ET) consists of three components, i.e., canopy transpiration, interception, and evaporation from the ground surface. Vegetation transpiration is calculated using a semi-mechanistic model of stomatal conductance (Ball et al., 1986), which is coupled with canopy carbon assimilation and water exchange between a leaf and the boundary layer to give

$$g_{s,h_2o} = \frac{mA_n}{C_s} h_s + b \quad (1)$$

where A_n is the net photosynthesis rate at leaf level (μmol CO_2 m^{-2} s^{-1}), $g_{s,h2o}$ is the leaf-level stomatal conductance of water vapor (μmol H_2O m^{-2} s^{-1}), C_s is the CO_2 concentration (μmol μmol^{-1}) at the leaf surfaces, h_s is the relative humidity at the leaf surface (%), and m and b are empirical parameters.

IBIS represents natural vegetation using PFTs, based on the biomass and leaf area index. Overall, 12 PFTs are defined in IBIS, related to bioclimatic limits, and physiological, morphological, phenological, and life-history criteria governing competition for light and water (Alton, 2011). Different physiological parameters are set for each PFT to quantify factors such as the phenological performance or carbon assimilation and water consumption characteristics (Kucharik et al., 2000). As a result, GPP and thus net primary production (NPP) and vegetation transpiration, are calculated separately for upper (trees) and lower (shrublands and grass) canopies as

$$NPP = (1-\eta)\int (A_g - R_{leaf} - R_{stem} - R_{root})dt \quad (2)$$

where A_g is the gross canopy production, η is the fraction of carbon lost by growth respiration (fixed value of 0.3), and R_{leaf}, R_{stem}, and R_{root} are leaf, stem, and root

143 respiration, respectively.

144 The model allows for the coexistence of different PFTs in a single grid cell.
145 However, a dynamic vegetation mechanism is used to simulate annual changes in
146 vegetation structure through PFT competition for light, water, and other nutrient
147 resource pools (Kucharik et al., 2006). The competition among PFTs is driven by
148 differences among carbon balances resulting from phenology, leaf form, and
149 photosynthetic pathways (Foley et al., 1996; Kucharik et al., 2000). On the annual
150 scale, the NPP is allocated among three carbon pools, i.e., leaves, stems (for trees),
151 and roots. The instantaneous change in the biomass pool *j* of PFT *i* is represented as

152 $$\frac{\partial C_{i,j}}{\partial t} = a_{i,j} NPP_i - \frac{C_{i,j}}{\tau_{i,j}} \quad (3)$$

153 where $a_{i,j}$ is the fraction of annual NPP allocated to the biomass pool and $\tau_{i,j}$ is the
154 carbon residence time of that biomass pool. Note that $a_{i,j}$ is a fixed value in IBIS, but
155 in some other DGVMs (e.g., the Lund–Potsdam–Jena dynamic global vegetation
156 model, Sitch et al., 2003) the NPP is allocated using allometric equations.

157 A relatively simple phenology module based on accumulated growing degree
158 days (GDD, Botta et al., 2000) is used in the original IBIS. A modified version of the
159 phenology scheme, based on that reported by Jolly et al. (2005), was developed in this
160 study. In detail, the prognostic phenology model is based on the growing season index
161 (GSI), which is decided by three main environmental factors, i.e., temperature,
162 photoperiod, and humidity (Equation 4). The photoperiod is calculated according to
163 the latitude of the model grid and empirical algorithms. We also adopted a 21-day
164 running mean GSI calculated from daily mean meteorological variables, following
165 Jolly et al. (2005).

166 $$GSI = f(\overline{T_m}) \times f(\overline{R_g}) \times f(\overline{VPD}) \quad (4)$$

where T_m, R_g, and VPD are multi-day running mean averages of air temperature (℃), solar radiation (W m^{-2}) and vapor pressure deficit (Pa); $f\left(\overline{Tm}\right)$, $f\left(\overline{Rg}\right)$, and $f\left(\overline{VPD}\right)$ vary linearly between the constraining limits 0 and 1, and thus regulate vegetation activity; these functions are defined in Equations (2–4) in Stöckli et al. (2008). The performance of the GSI phenology model would be evaluated by the moderate-resolution imaging spectoradiometer (MODIS) leaf area index (LAI, m^2 m^{-2}) products (MOD15A2, Myneni et al., 1997) for two deciduous forest sites in the following analysis.

2.2 Model input data

In the present study, IBIS was executed globally at a $0.5° \times 0.5°$ latitude–longitude grid resolution. The initial vegetation type was obtained from MODIS MOD12Q1 product (Friedl et al., 2010), and resampled to 0.5°. Soil texture data were obtained from the Center for Sustainability and the Global Environment (http://www.sage.wisc.edu/download/IBIS/ibis.html), and was reformatted from the Global Soil Data Products CD-ROM issued by the International Geosphere–Biosphere Programme Data and Information Services. The topographical data were obtained from the Shuttle Radar Topographic Mission (http://srtm.usgs.gov/), with a resolution of 1000 m. We resampled the resolution to 0.5 °(~ 50 km) as a model grid.

The climate data, including monthly mean air temperature, precipitation, relative humidity, cloudiness, diurnal temperature range, wind speed, and the number of wet days, were obtained from the Climate Research Unit (CRU) climate dataset for 1901 through 2010 (CRUTS3.10, Harris et al. 2014, hereafter CRU). We examined the modeled biomass uncertainty induced by different meteorological datasets using forcing data from Princeton University (http://hydrology.princeton.edu/data.pgf.php, hereafter Princeton forcing data) to drive the model. Princeton forcing data does not

include wind speed; therefore we use the wind speed data from the Global Land Data Assimilation System covering the period 1948–2010 (http://disc.sci.gsfc.nasa.gov/services/grads-gds/gldas). The Princeton forcing data was developed at a global spatial scale of 0.5 °, with a daily timescale. In both cases, we spun-up the model for 190 years (1759-1948) and then conducted transient simulations starting from 1948, and climate data in 1901were used for the years before this year.

2.3 Model calibration and improvements

We collected site-level GPP data from Fluxnet (http://fluxnet.ornl.gov/) to calibrate the IBIS model. Only sites with at least 2-year data were collected, because there may be greater uncertainty for sites that cover shorter than 2 years. Overall, 39 sites were selected, covering tropical, temperate, and boreal forests, and grasslands or croplands (Fig. S1, Table S1). Note that IBIS does not simulate croplands explicitly; therefore croplands were compared with the simulation results for the understory. The calibration was conducted at both monthly and annul scales.

To constrain the model with both flux and biometric data, we also collected plot-level AGB data from the literature. In this study, we mainly collected plot measurements of AGB from papers published between 1980 and 2010 (Fig. S1, Table S2). The allometric equations used in these literatures were based on either DBH (diameter at breast height) or DBH and tree height. To ensure the in-situ plot measurements were representative to the forest conditions of corresponding locations, the collected plot measurements were further filtered to ensure they were larger than 0.05 ha in size. The records measured through harvesting methods were also excluded from the AGB estimation procedures. In total of 992 plot samples were retained in this study for the model calibration. The resolution of plot-level data is usually 0.01 °,

therefore we used the average value as a proxy for a model grid. Note that the model calculates the carbon density (Mg C ha^{-1}) instead of AGB, therefore we calculated AGB (Mg ha^{-1}) by multiplying by a commonly-used factor of 2.0 (IPCC, 2003).

To minimize the number of parameters for calibration, default values provided by Foley et al. (1996) and Kucharik et al. (2000) were used for most parameters. We calibrated parameters the most sensitive to GPP and AGB (Table 1). We mainly calibrated the photosynthesis capacity at 15 ℃ (vmax_pft) for different PFTs, as in Castanho et al. (2013). The flux data were mainly for boreal and temperate forests and grassland (including crops), because of the data gaps for tropical forest. We therefore used the parameters derived from literature for tropical forest (Zhu et al., 2011). The parameters were manually calibrated by a try and error method to constrain the model simulation of GPP and AGB to match the observations for most sites. Furthermore, we showed the model simulations with default parameters in Kucharik et al. (2000) as a baseline run to evaluate the model improvements after calibration (calibrated run).

To illustrate how spatial heterogeneous parameter can improve model simulation, we generated a regional woody residence time (τ_w, years) gridded map, which was proved to be sensitive to AGB, for pan-tropical forests.The exploration of τ_w was conducted by the Random Forest method (Breiman, 2001), based on collected τ_w data (Table S3) and five ancillary predictors of mean annual temperature, annual precipitation, GPP, evapotranspiration (ET) and DEM. The Random Forest extrapolation method was implemented based on the "randomForest" R package (Liaw and Wiener, 2002), which includes both classification and regression functions. Long-term climatological temperature and precipitation data (1950–2005) were obtained from WorldClim (http://www.worldclim.org/) with a resolution of 1 km. The GPP and ET datasets (1 km resolution) were both available from the Numerical

Terradynamic Simulation Group website (http://www.ntsg.umt.edu/biblio). The DEM data used were obtained from the NASA Shuttle Radar Topographic Mission with a resolution of 90 m (http://srtm.csi.cgiar.org/). The resulted pan-tropical τ_w gridded map was in 1 km resolution and was resampled to 0.5 °for model simulation.

3 Results

3.1 Phenology model

We compared the model simulated LAI by the IBIS default (GDD) and GSI phenology models with MODIS values for two forest sites (Fig. 1). Both of the two phenology models can generally reproduce the LAI seasonal variation, even though lower values in dormancy season are overestimated for the boreal site. For both sites, GDD model results in a longer growing season compared with GSI model and MODIS observations. This may induce overestimated GPP for the model simulations.

3.2 Calibration by GPP

The model performs well for most sites after calibration (Table 2). All of the forest sites have determination coefficients (R^2) above 0.6 for GPP at the monthly scale except for US-Goo and US-SP2. The model simulates upper canopy (forests) better than lower canopy (shrubs and grasses), with large R^2 and small deviations from 1 for the GPP slope (Table 2).

At the annual-scale, there are strong correlations between the model simulated and in situ GPP for both baseline and calibrated runs (Fig. 2). In both runs, the simulations slightly overestimate small values and underestimate large values compared with the in situ observations. When GPP were below 500 gC m^{-2} $year^{-1}$, the simulated GPP are around twice the observed values. This systematic error may be caused by the overestimated LAI from both of the two phenology models (Fig. 1). Compared with the baseline run, the calibrated model reduces the root mean square

error (RMSE) from 599.3 to 522.9 gC m^{-2} $year^{-1}$.

3.3 Calibration by plot-level biomass

Fig. 3 shows a comparison of the modeled biomass with plot-level observations for baseline and calibration runs. Each point shows a pair of values from a certain simulated IBIS grid and an averaged value of all the plots within this grid. The simulations show significant correlations in both cases but with overestimated low values and underestimated large ones. The baseline run cannot reproduce the large biomass when it is above 300 Mg ha^{-1}. In comparison, the calibrated run improves the simulation for large AGB; but was also subjected to widely scattering. The large scattering for both runs may be caused by the difference in spatial resolution between the site location (0.01 °) and the model grid (0.5 °). Furthermore, both model runs use only one parameter to represent a PFT; while in reality, spatial patterns of these parameters are heterogeneous (see below).

3.4 Global and regional AGB

Using the calibrated parameters, we simulate the spatial pattern of global AGB (upper and under layers, Fig. 4a). The global average biomass is 81.73 Mg ha^{-1}, with the largest values in tropical areas and the lowest in boreal areas. The global map of AGB shows large heterogeneity, which is similar to the case for global GPP patterns. The zonal AGB within each 0.5 ° latitude interval shows a large fluctuation (Fig. 4b). Two maxima of 278.44 and 112.17 Mg ha^{-1} are found around 1.25 ° S and 56.25 ° N, respectively when model is driven by Princeton forcing data. AGB differences induced by the two meteorological forcing data are small.

Based on the collected τ_w, we generate a pan-tropical gridded τ_w map by integrating other variables as predictive variables of the Random Forest method. τ_w exhibits large spatial heterogeneity, with an average value of 55.8 years over the

pan-tropical forests (Fig. 5a). Large values of τ_w are found in eastern Amazonian forest areas and Bornean tropical rainforests. Areas with a large τ_w also exhibit a large degree of uncertainty (Fig. 5b).The estimated τ_w values in Amazonian forests show a west–east increasing gradient as highlighted by other authors (Galbraith *et al*., 2013). Correspondingly, the model simulation of AGB with the gridded τ_w map also shows a west–east increasing gradient compared with the results by calibrated τ_w (Fig. 5c). The estimated τ_w for central African forests has a moderate value of about 40 years with lower simulated AGB accordingly.

The model performance of simulated AGB with 'default', calibrated and our estimated τ_w for tropical forests plots are also compared (Fig. 6). Each point in Fig. 6 indicates one or more plots that are located in the same IBIS grid ($0.5° \times 0.5°$). The simulated AGB using default τ_w showed large scattering, with underestimation for large amounts of AGB. Actually, the default τ_w resulted in many small amounts of AGB (close to 0), which indicates a wrong PFT for the model simulation. The calibrated model run improves compared with baseline run; but is still with large scattering and RMSE (73.1 Mg ha^{-1}). The resulting AGB from the improved τ_w has a relatively close relationship with plot values, even though underestimation can still be observed when AGB is above 400 Mg ha^{-1} (Fig. 6c). Compared with the results from the calibrated run, the RMSE of AGB is reduced to 55.4 Mg ha^{-1} when model uses the estimated τ_w.

Four Fluxnet sites, representing different woody PFTs, were randomly selected to test the AGB uncertainties due to τ_w (Table 2, Fig. 7). Five hundred τ_w values were randomly chosen between the default and calibrated values using the Monte Carlo method. The simulated AGB is shown to be sensitive to τ_w for all sites, resulting in a large variation in τ_w by the year of 2010. All the sites show an increasing trend during

the test runs, except for the tropical deciduous site (Au-How). Variations in AGB are around 50 Mg ha^{-1} by 2010 for the two temperate PFTs (Us-Me2 and US-Ha1), indicating large uncertainties caused by τ_w. This further reveals the necessity to accurate estimate τ_w for model simulation.

3.5 Global AGB driven by CRU metrological data

Fig. 8 displays the spatial pattern of the difference between AGB driven by Princeton forcing data and CRU data. Most areas of the globe show AGB differences within 20 Mg ha^{-1} (averaged as 12.83) according to the two meteorological datasets. Large differences are observed in savanna regions (MODIS UMD classification scheme) in South America and central Africa, and shrublands in northeastern Siberia (Fig. 8). In these areas, the AGB driven by daily meteorological data (Princeton forcing data) is significantly larger than those derived from CRU data. In contrast, in most tropical areas, the AGB derived from Princeton forcing dataset is smaller than those derived from CRU datasets. Most of the grids show a relative error within ±20% with largest frequency occurs for relative error of 10 % (data not shown).

4 Discussion

4.1 Estimation of AGB

We used a single set of model parameters to estimate the global carbon stock in terms of AGB. The IBIS model does not calculate the global AGB directly, but calculates the carbon density. We therefore compared our model-derived carbon density with those from other studies. Our model-derived carbon density is smaller than that reported by Pan et al. (2011) on the global scale (82.96 compared with 94.2 Mg C ha^{-1}), and this results in a smaller global carbon stock (Table 3). Pan et al. (2011) calculated the carbon density, using the forest inventory method, for the period 1990–2007; their estimated value of 94.2 Mg C ha^{-1} includes both above- and

342 below-ground biomass. Previous research showed that ~80% of the total biomass is in
343 AGB and ~20% is in below-ground biomass for forest ecosystems on the global scale
344 (Cairns et al., 1997). This indicates that the global above-ground carbon density is
345 ~75 Mg C ha^{-1} for Pan et al. (2011). This value is comparable to our modeling result.
346 The difference between the global carbon stocks in AGB may arise from the different
347 forest areas used by Pan et al. (2011) and in our study (MODIS derived). The forest
348 areas were 3851.3 $\times 10^6$ and 3332.35 $\times 10^6$ ha in Pan et al.'s study and our study,
349 respectively. Further comparisons of the regional-scale carbon density with those
350 from three other studies show that values in our study and those reported by Pan et al.
351 (2011) are larger. The carbon densities reported by Goodale et al. (2002) and Liski et
352 al. (2003) are around 30% smaller than those reported by Thurner et al. (2014) and in
353 our study for European forests. In contrast, for North American forests, the carbon
354 densities reported by Pan et al. (2011) and in our study are similar, and larger than
355 those in the other three studies. These comparisons with other studies show that the
356 IBIS-model-derived carbon density gives reasonable results on the global scale and
357 can therefore be used as an independent tool for validating AGB estimations by other
358 methods.

359 **4.2 Influences of woody residence time on modeled AGB**

360 A comparison of the observed and modeled AGB for pan-tropical forests shows
361 that the spatial patterns in the modeling results are biased (Figs. 5 and 6). Though our
362 plot-level calibration shows a significant relationship between modeled and plot level
363 data, the calibration points are subject to scatter. The calibration results shows that the
364 model tends to underestimate AGB when AGB is large (Figs. 3 and 6). Similar R^2
365 values were reported by Seiler et al. (2013) for a regional-scale model calibration in
366 Bolivia. The calibration results indicate that a single value of τ_w in the model cannot

reproduce the spatial variance of AGB in a large scale. When estimated gridded τ_w for pan-tropical forests was used for model simulation, the resulted AGB improves with a smaller RMSE (Figs. 5 and 6). Similar research by Castanho et al. (2013) showed that the woody residence time is the most important parameter in determining the spatial variance in modeled AGB in this area. Further investigation using a spatial pattern of τ_w in IBIS greatly improved the modeled AGB, with R^2 changing from 0.33 to 0.88 (Castanho et al., 2013). These and the presented results indicate that to improve the model simulation accuracy, modelers should consider the spatial heterogeneity of the most important parameters in the model used, especially for large-scale simulations.

4.3 Influences of meteorological data on modeled AGB

Climate-data-driven uncertainties in modeling carbon and energy cycles have previously been analyzed (Zhao et al., 2005; Barman et al., 2014a, b). A systematic analysis based on various global vegetation models and meteorological data showed that substantial changes in the modeled GPP were observed for different meteorological inputs in regional simulations in Europe (Jung et al., 2007). Substantial differences in GPP were observed by different meteorological drivers. A similar analysis by Barman et al. (2014b) showed that the differences in site-level GPP caused by different meteorological drivers were ~20% of the annual GPP. This was mainly caused by biases in short-wave radiation and humidity for various meteorological drivers tested in the study. The relative differences caused by different climate drivers are generally within ±20% in this study (data not shown). These differences are smaller than the relative errors induced by the invariant parameters over the pan-tropical forest. This indicates that to improve the model simulation accuracy, modelers should pay attention to both model parameter calibration and metrological drivers, with a focus on the former.

Data availability is one of the main reasons that few global model simulations use plot-level data to constrain the model (Seiler et al., 2014). We collected plot-level AGB data from the literature, and used them to calibrate and validate IBIS on the global scale. The plot resolution was generally 0.01–0.1 ° (~1–10 km). In the validation, we used measured single-point values as a proxy for a model grid average (~2500 km^2), which may have caused a bias relative to the modeled values. Note that even over a small area, AGB may vary greatly because of local soil type, land use variability, and local water availability (Baker et al., 2004). Therefore, the difference between the spatial scales of the plot level and our model simulation grid may partly explain the small R^2 in Fig. 3. Further investigations of model simulations at different spatial resolution (especially at high resolution) are therefore necessary to facilitate model calibration by higher spatial resolution AGB datasets. Furthermore, the plot points used for calibration are from natural forests, with little human disturbance, therefore our modeling results represent the potential value under current climate conditions (e.g., Mu et al., 2008; Seiler et al., 2014). AGB in Table 3 are present-day value as in the original researches, which may be influenced by human activities. A direct comparison of model simulation with these data is therefore to some extent inappropriate. However, this comparison is useful, because based on exploration of the difference between the two, the model could be used to quantify the impact of human activities (such as land use change, deforestation, or afforestation) on large-scale AGB change.

5 Conclusions

In this study, we evaluated the model performance in simulating global carbon dynamics. IBIS, which was calibrated using in situ GPP and plot-level AGB data collected from the literature, was used as an example to perform the comparison.

Calibration results showed that IBIS can reproduce GPP with acceptable accuracies at the site and global levels. In the global-scale, the IBIS simulated total AGB gave results similar to those obtained in other studies. However, discrepancies in spatial patterns were observed between model-derived and observed AGB mainly because of the single parameter set used in the model. Two metrological datasets, i.e., Princeton forcing data and CRU data, were used to test the model uncertainties caused by climate drivers. The results indicated that the two meteorological inputs resulted in substantially different global-scale AGB estimations, although this difference was small compared to the parameter-induced difference. The conclusions of our research highlight the necessity of considering the heterogeneity of key model physiological parameters in modeling global AGB. The research also shows that to simulate large-scale carbon dynamics, both carbon flux and AGB data are necessary to constrain the model. The main conclusions of our research could help to improve model simulation of the global carbon cycle.

Acknowledgements

This study was financially supported by the National Science Foundation of China (Grant No. 41301020) and the National Key Basic Research Program of China (2013CB956604). We are grateful to the PIs and Co-Is of FLUXNET who make their data freely available to the ecological modelling community through the FLUXNET archive (http://fluxnet.ornl.gov/), in particular by the following networks: AmeriFlux (U.S. Department of Energy, Biological and Environmental Research, Terrestrial Carbon Program (DE-FG02-04ER63917 and DE-FG02-04ER63911)), AfriFlux, AsiaFlux, CarboAfrica, CarboEuropeIP, CarboItaly, CarboMont, ChinaFlux, Fluxnet-Canada (supported by CFCAS, NSERC, BIOCAP, Environment Canada,

and NRCan), GreenGrass, KoFlux, LBA, NECC, OzFlux, TCOS-Siberia, USCCC. We acknowledge the financial support to the eddy covariance data harmonization provided by CarboEuropeIP, FAO-GTOS-TCO, iLEAPS, Max Planck Institute for Biogeochemistry, National Science Foundation, University of Tuscia, Universit é Laval, Environment Canada and US Department of Energy and the database development and technical support from Berkeley Water Center, Lawrence Berkeley National Laboratory, Microsoft Research eScience, Oak Ridge National Laboratory, University of California – Berkeley and the University of Virginia.

References

Alton, P. B.: How useful are plant functional types in global simulations of the carbon, water, and energy cycles?, Journal of Geophysical Research-Biogeosciences, 116, 2011.

Asner, G. P., Powell, G. V. N., Mascaro, J., Knapp, D. E., Clark, J. K., Jacobson, J., Kennedy-Bowdoin, T., Balaji, A., Paez-Acosta, G., Victoria, E., Secada, L., Valqui, M., and Hughes, R. F.: High-resolution forest carbon stocks and emissions in the Amazon, Proceedings of the National Academy of Sciences of the United States of America, 107, 16738-16742, 2010.

Baker, T. R., Phillips, O. L., Malhi, Y., Almeida, S., Arroyo, L., Di Fiore, A., Erwin, T., Killeen, T. J., Laurance, S. G., Laurance, W. F., Lewis, S. L., Lloyd, J., Monteagudo, A., Neill, D. A., Patino, S., Pitman, N. C. A., Silva, J. N. M., and Martinez, R. V.: Variation in wood density determines spatial patterns in Amazonian forest biomass, Global Change Biology, 10, 545-562, 2004.

Ball J.T., W. I. E. a. B. J. A.: A model predicting stomatal conductance and its contribution to the control of photosynthesis under different environmental conditions. J., B. (Ed.), Springer, New York, 1987.

Barman, R., Jain, A. K., and Liang, M.: Climate-driven uncertainties in modeling terrestrial energy and water fluxes: a site-level to global-scale analysis, Global Change Biology, 20, 1885-1900, 2014a.

Barman, R., Jain, A. K., and Liang, M.: Climate-driven uncertainties in modeling terrestrial gross primary production: a site level to global-scale analysis, Global Change Biology, 20, 1394-1411, 2014b.

Beer, C., Reichstein, M., Tomelleri, E., Ciais, P., Jung, M., Carvalhais, N.,

475 Roedenbeck, C., Arain, M. A., Baldocchi, D., Bonan, G. B., Bondeau, A.,
476 Cescatti, A., Lasslop, G., Lindroth, A., Lomas, M., Luyssaert, S., Margolis, H.,
477 Oleson, K. W., Roupsard, O., Veenendaal, E., Viovy, N., Williams, C., Woodward,
478 F. I., and Papale, D.: Terrestrial Gross Carbon Dioxide Uptake: Global
479 Distribution and Covariation with Climate, Science, 329, 834-838, 2010.
480 Botta, A., Viovy, N., Ciais, P., Friedlingstein, P., and Monfray, P.: A global prognostic
481 scheme of leaf onset using satellite data, Global Change Biology, 6, 709-725,
482 2000.
483 Breiman, L.: Random forests, Machine Learning, 45, 5-32, 2001.
484 Cairns, M. A., Brown, S., Helmer, E. H., and Baumgardner, G. A.: Root biomass
485 allocation in the world's upland forests, Oecologia, 111, 1-11, 1997.
486 Castanho, A. D. A., Coe, M. T., Costa, M. H., Malhi, Y., Galbraith, D., and Quesada,
487 C. A.: Improving simulated Amazon forest biomass and productivity by
488 including spatial variation in biophysical parameters, Biogeosciences, 10,
489 2255-2272, 2013.
490 Cramer, W., Bondeau, A., Woodward, F. I., Prentice, I. C., Betts, R. A., Brovkin, V.,
491 Cox, P. M., Fisher, V., Foley, J. A., Friend, A. D., Kucharik, C., Lomas, M. R.,
492 Ramankutty, N., Sitch, S., Smith, B., White, A., and Young-Molling, C.: Global
493 response of terrestrial ecosystem structure and function to CO2 and climate
494 change: results from six dynamic global vegetation models, Global Change
495 Biology, 7, 357-373, 2001.
496 Delbart, N., Ciais, P., Chave, J., Viovy, N., Malhi, Y., and Le Toan, T.: Mortality as a
497 key driver of the spatial distribution of aboveground biomass in Amazonian
498 forest: results from a dynamic vegetation model, Biogeosciences, 7, 3027-3039,
499 2010.

500 Dixon, R. K., Brown, S., Houghton, R. A., Solomon, A. M., Trexler, M. C., and
501 Wisniewski, J.: CARBON POOLS AND FLUX OF GLOBAL FOREST
502 ECOSYSTEMS, Science, 263, 185-190, 1994.
503 Foley, J. A., Prentice, I. C., Ramankutty, N., Levis, S., Pollard, D., Sitch, S., and
504 Haxeltine, A.: An integrated biosphere model of land surface processes,
505 terrestrial carbon balance, and vegetation dynamics, Global Biogeochemical
506 Cycles, 10, 603-628, 1996.
507 Friedl, M. A., Sulla-Menashe, D., Tan, B., Schneider, A., Ramankutty, N., Sibley, A.,
508 and Huang, X.: MODIS Collection 5 global land cover: Algorithm refinements
509 and characterization of new datasets, Remote Sensing of Environment, 114,
510 168-182, 2010.
511 Galbraith, D., Levy, P. E., Sitch, S., Huntingford, C., Cox, P., Williams, M., and Meir,
512 P.: Multiple mechanisms of Amazonian forest biomass losses in three dynamic
513 global vegetation models under climate change, New Phytologist, 187, 647-665,
514 2010.
515 Goodale, C. L., Apps, M. J., Birdsey, R. A., Field, C. B., Heath, L. S., Houghton, R.
516 A., Jenkins, J. C., Kohlmaier, G. H., Kurz, W., Liu, S. R., Nabuurs, G. J., Nilsson,
517 S., and Shvidenko, A. Z.: Forest carbon sinks in the Northern Hemisphere,
518 Ecological Applications, 12, 891-899, 2002.
519 Harris, I., Jones, P. D., Osborn, T. J., and Lister, D. H.: Updated high-resolution grids
520 of monthly climatic observations – the CRU TS3.10 Dataset, International
521 Journal of Climatology, 34, 623-642, 2014.
522 Huntingford, C., Fisher, R. A., Mercado, L., Booth, B. B. B., Sitch, S., Harris, P. P.,
523 Cox, P. M., Jones, C. D., Betts, R. A., Malhi, Y., Harris, G. R., Collins, M., and
524 Moorcroft, P.: Towards quantifying uncertainty in predictions of Amazon

525 'dieback', Philosophical Transactions of the Royal Society B-Biological Sciences,
526 363, 1857-1864, 2008.
527 Huntingford, C., Zelazowski, P., Galbraith, D., Mercado, L. M., Sitch, S., Fisher, R.,
528 Lomas, M., Walker, A. P., Jones, C. D., Booth, B. B. B., Malhi, Y., Hemming, D.,
529 Kay, G., Good, P., Lewis, S. L., Phillips, O. L., Atkin, O. K., Lloyd, J., Gloor, E.,
530 Zaragoza-Castells, J., Meir, P., Betts, R., Harris, P. P., Nobre, C., Marengo, J.,
531 and Cox, P. M.: Simulated resilience of tropical rainforests to CO2-induced
532 climate change, Nature Geoscience, 6, 268-273, 2013.
533 IPCC (Intergovernmental Panel on Climate Change). Good practice guidance for land
534 use, land-use change and forestry (ed. J. Penman, M. Gytarsky, T. Hiraishi, T.
535 Krug, D. Kruger, R. Pipatti, L. Buendia, K. Miwa, T. Ngara, K. Tanabeand, and
536 F. Wagner), pp. 3.14–G.9. Institute for Global Environmental Strategies:
537 Kanagawa, Japan, 2003.
538 Jolly, W. M., Nemani, R., and Running, S. W.: A generalized, bioclimatic index to
539 predict foliar phenology in response to climate, Global Change Biology, 11,
540 619-632, 2005.
541 Jung, M., Vetter, M., Herold, M., Churkina, G., Reichstein, M., Zaehle, S., Ciais, P.,
542 Viovy, N., Bondeau, A., Chen, Y., Trusilova, K., Feser, F., and Heimann, M.:
543 Uncertainties of modeling gross primary productivity over Europe: A systematic
544 study on the effects of using different drivers and terrestrial biosphere models,
545 Global Biogeochemical Cycles, 21, 2007.
546 Keith, H., Mackey, B. G., and Lindenmayer, D. B.: Re-evaluation of forest biomass
547 carbon stocks and lessons from the world's most carbon-dense forests,
548 Proceedings of the National Academy of Sciences of the United States of
549 America, 106, 11635-11640, 2009.

Kindermann, G., Obersteiner, M., Sohngen, B., Sathaye, J., Andrasko, K., Rametsteiner, E., Schlamadinger, B., Wunder, S., and Beach, R.: Global cost estimates of reducing carbon emissions through avoided deforestation, Proceedings of the National Academy of Sciences of the United States of America, 105, 10302-10307, 2008.

Kondo, M., Ichii, K., Ueyama, M., Mizoguchi, Y., Hirata, R., and Saigusa, N.: The role of carbon flux and biometric observations in constraining a terrestrial ecosystem model: a case study in disturbed forests in East Asia, Ecological Research, 28, 893-905, 2013.

Kucharik, C. J., Foley, J. A., Delire, C., Fisher, V. A., Coe, M. T., Lenters, J. D., Young-Molling, C., Ramankutty, N., Norman, J. M., and Gower, S. T.: Testing the performance of a Dynamic Global Ecosystem Model: Water balance, carbon balance, and vegetation structure, Global Biogeochemical Cycles, 14, 795-825, 2000.

Lefsky, M. A., Harding, D. J., Keller, M., Cohen, W. B., Carabajal, C. C., Espirito-Santo, F. D., Hunter, M. O., and de Oliveira, R.: Estimates of forest canopy height and aboveground biomass using ICESat, Geophysical Research Letters, 32, 2005.

Liaw, A. and Wiener, M. 2002. Classification and regression by randomForest. *R news*, **2**, 18-22,2002.

Liski, J., Korotkov, A. V., Prins, C. F. L., Karjalainen, T., Victor, D. G., and Kauppi, P. E.: Increased carbon sink in temperate and boreal forests, Climatic Change, 61, 89-99, 2003.

Luyssaert, S., Inglima, I., Jung, M., Richardson, A. D., Reichstein, M., Papale, D., Piao, S. L., Schulzes, E. D., Wingate, L., Matteucci, G., Aragao, L., Aubinet, M.,

575 Beers, C., Bernhofer, C., Black, K. G., Bonal, D., Bonnefond, J. M., Chambers,
576 J., Ciais, P., Cook, B., Davis, K. J., Dolman, A. J., Gielen, B., Goulden, M.,
577 Grace, J., Granier, A., Grelle, A., Griffis, T., Gruenwald, T., Guidolotti, G.,
578 Hanson, P. J., Harding, R., Hollinger, D. Y., Hutyra, L. R., Kolar, P., Kruijt, B.,
579 Kutsch, W., Lagergren, F., Laurila, T., Law, B. E., Le Maire, G., Lindroth, A.,
580 Loustau, D., Malhi, Y., Mateus, J., Migliavacca, M., Misson, L., Montagnani, L.,
581 Moncrieff, J., Moors, E., Munger, J. W., Nikinmaa, E., Ollinger, S. V., Pita, G.,
582 Rebmann, C., Roupsard, O., Saigusa, N., Sanz, M. J., Seufert, G., Sierra, C.,
583 Smith, M. L., Tang, J., Valentini, R., Vesala, T., and Janssens, I. A.: CO2 balance
584 of boreal, temperate, and tropical forests derived from a global database, Global
585 Change Biology, 13, 2509-2537, 2007.
586 Malhi, Y., Phillips, O. L., Lloyd, J., Baker, T., Wright, J., Almeida, S., Arroyo, L.,
587 Frederiksen, T., Grace, J., Higuchi, N., Killeen, T., Laurance, W. F., Leano, C.,
588 Lewis, S., Meir, P., Monteagudo, A., Neill, D., Vargas, P. N., Panfil, S. N., Patino,
589 S., Pitman, N., Quesada, C. A., Rudas-Ll, A., Salomao, R., Saleska, S., Silva, N.,
590 Silveira, M., Sombroek, W. G., Valencia, R., Martinez, R. V., Vieira, I. C. G., and
591 Vinceti, B.: An international network to monitor the structure, composition and
592 dynamics of Amazonian forests (RAINFOR), Journal of Vegetation Science, 13,
593 439-450, 2002.
594 McGuire, A. D., Sitch, S., Clein, J. S., Dargaville, R., Esser, G., Foley, J., Heimann,
595 M., Joos, F., Kaplan, J., Kicklighter, D. W., Meier, R. A., Melillo, J. M., Moore,
596 B., Prentice, I. C., Ramankutty, N., Reichenau, T., Schloss, A., Tian, H., Williams,
597 L. J., and Wittenberg, U.: Carbon balance of the terrestrial biosphere in the
598 twentieth century: Analyses of CO2, climate and land use effects with four
599 process-based ecosystem models, Global Biogeochemical Cycles, 15, 183-206,

2001.

Mu, Q., Zhao, M., Running, S. W., Liu, M., and Tian, H.: Contribution of increasing CO(2) and climate change to the carbon cycle in China's ecosystems, Journal of Geophysical Research-Biogeosciences, 113, 2008.

Myneni, R. B., Nemani, R. R., and Running, S. W.: Estimation of global leaf area index and absorbed par using radiative transfer models, Ieee Transactions on Geoscience and Remote Sensing, 35, 1380-1393, 1997.

Pan, Y., Birdsey, R. A., Fang, J., Houghton, R., Kauppi, P. E., Kurz, W. A., Phillips, O. L., Shvidenko, A., Lewis, S. L., Canadell, J. G., Ciais, P., Jackson, R. B., Pacala, S. W., McGuire, A. D., Piao, S., Rautiainen, A., Sitch, S., and Hayes, D.: A Large and Persistent Carbon Sink in the World's Forests, Science, 333, 988-993, 2011.

Purves, D. and Pacala, S.: Predictive Models of Forest Dynamics, Science, 320, 1452-1453, 2008.

Saatchi, S. S., Harris, N. L., Brown, S., Lefsky, M., Mitchard, E. T. A., Salas, W., Zutta, B. R., Buermann, W., Lewis, S. L., Hagen, S., Petrova, S., White, L., Silman, M., and Morel, A.: Benchmark map of forest carbon stocks in tropical regions across three continents, Proceedings of the National Academy of Sciences of the United States of America, 108, 9899-9904, 2011.

Seiler, C., Hutjes, R. W. A., Kruijt, B., Quispe, J., Anez, S., Arora, V. K., Melton, J. R., Hickler, T., and Kabat, P.: Modeling forest dynamics along climate gradients in Bolivia, Journal of Geophysical Research-Biogeosciences, 119, 758-775, 2014.

Sitch, S., Huntingford, C., Gedney, N., Levy, P. E., Lomas, M., Piao, S. L., Betts, R., Ciais, P., Cox, P., Friedlingstein, P., Jones, C. D., Prentice, I. C., and Woodward, F. I.: Evaluation of the terrestrial carbon cycle, future plant geography and climate-carbon cycle feedbacks using five Dynamic Global Vegetation Models

(DGVMs), Global Change Biology, 14, 2015-2039, 2008.

Sitch, S., Smith, B., Prentice, I. C., Arneth, A., Bondeau, A., Cramer, W., Kaplan, J. O., Levis, S., Lucht, W., Sykes, M. T., Thonicke, K., and Venevsky, S.: Evaluation of ecosystem dynamics, plant geography and terrestrial carbon cycling in the LPJ dynamic global vegetation model, Global Change Biology, 9, 161-185, 2003.

Stöckli, R., Rutishauser, T., Dragoni, D., O'Keefe, J., Thornton, P. E., Jolly, M., Lu, L., and Denning, A. S.: Remote sensing data assimilation for a prognostic phenology model, Journal of Geophysical Research: Biogeosciences, 113, n/a-n/a, 2008.

Tao, S., Guo, Q., Li, L., Xue, B., Kelly, M., Li, W., Xu, G., and Su, Y.: Airborne Lidar-derived volume metrics for aboveground biomass estimation: A comparative assessment for conifer stands, Agricultural and Forest Meteorology, 198, 24-32, 2014.

Thompson, S. L. and Pollard, D.: A GLOBAL CLIMATE MODEL (GENESIS) WITH A LAND-SURFACE TRANSFER SCHEME (LSX) .1. PRESENT CLIMATE SIMULATION, Journal of Climate, 8, 732-761, 1995a.

Thompson, S. L. and Pollard, D.: A GLOBAL CLIMATE MODEL (GENESIS) WITH A LAND-SURFACE TRANSFER SCHEME (LSX) .2. CO2 SENSITIVITY, Journal of Climate, 8, 1104-1121, 1995b.

Thurner, M., Beer, C., Santoro, M., Carvalhais, N., Wutzler, T., Schepaschenko, D., Shvidenko, A., Kompter, E., Ahrens, B., Levick, S. R., and Schmullius, C.: Carbon stock and density of northern boreal and temperate forests, Global Ecology and Biogeography, 23, 297-310, 2014.

Wolf, A., Ciais, P., Bellassen, V., Delbart, N., Field, C. B., and Berry, J. A.: Forest biomass allometry in global land surface models, Global Biogeochemical Cycles, 25, 2011.

650 Xiao, J., Davis, K. J., Urban, N. M., and Keller, K.: Uncertainty in model parameters
651 and regional carbon fluxes: A model-data fusion approach, Agricultural and
652 Forest Meteorology, 189, 175-186, 2014.
653 Xiao, J., Davis, K. J., Urban, N. M., Keller, K., and Saliendra, N. Z.: Upscaling
654 carbon fluxes from towers to the regional scale: Influence of parameter
655 variability and land cover representation on regional flux estimates, Journal of
656 Geophysical Research-Biogeosciences, 116, 2011.
657 Xue, B.-L., Kumagai, T. o., Iida, S. i., Nakai, T., Matsumoto, K., Komatsu, H., Otsuki,
658 K., and Ohta, T.: Influences of canopy structure and physiological traits on flux
659 partitioning between understory and overstory in an eastern Siberian boreal larch
660 forest, Ecological Modelling, 222, 1479-1490, 2011.
661 Zhao, M. S., Heinsch, F. A., Nemani, R. R., and Running, S. W.: Improvements of the
662 MODIS terrestrial gross and net primary production global data set, Remote
663 Sensing of Environment, 95, 164-176, 2005.
664 Zhu, Q., Jiang, H., Peng, C., Liu, J., Wei, X., Fang, X., Liu, S., Zhou, G., and Yu, S.:
665 Evaluating the effects of future climate change and elevated CO2 on the water
666 use efficiency in terrestrial ecosystems of China, Ecological Modelling, 222,
667 2414-2429, 2011.
668

669 ## Tables

670 **Table 1** Key PFT-dependent parameters for IBIS calibration. The abbreviations are defined as
671 follows: vmax_pft: maximum Rubisco capacity at top of canopy (μmol m^{-2} s^{-1}); SLA: specific
672 leaf area (m^2 kg^{-1}); τ_l: residence time of foliar biomass (years); τ_r: residence time of root biomass
673 (years); τ_w: residence time of wood biomass (years); a_{leaf}: allocation coefficient of total
674 photosynthate in foliar biomass (fraction); a_{root}: allocation coefficient of total photosynthate in root
675 biomass (fraction); a_{wood}: allocation coefficient of total photosynthate in wood biomass (fraction);
676 P_{min}: monthly minimum precipitation (mm $month^{-1}$); T_{minL}: absolute minimum temperature (lower
677 limit, ℃); T_{minU}: absolute minimum temperature (upper limit, ℃); T_{warm}: temperature of the
678 warmest month (℃) (C_4 plants only); GDD: minimum growing degree days above 5 ℃ threshold
679 for upper-canopy types; minimum growing degree days above 0 ℃ threshold for lower-canopy
680 types. The plant functional type (PFT) numbers defined in IBIS are as follows: 1, tropical
681 broadleaf evergreen trees; 2, tropical broadleaf drought-deciduous trees; 3, warm–temperate
682 broadleaf evergreen trees; 4, temperate conifer evergreen trees; 5, temperate broadleaf
683 cold-deciduous trees; 6, boreal conifer evergreen trees; 7, boreal broadleaf cold-deciduous trees; 8,
684 boreal conifer cold-deciduous trees; 9, evergreen shrubs; 10: cold-deciduous shrubs; 11, warm (C4)
685 grasses; and 12, cool (C3) grasses.

686

687

688

PFT	*vmax_pft*	*SLA*	τ_l	τ_r	τ_w	a_{leaf}	a_{root}	a_{wood}	P_{min}	T_{minL}	T_{minU}	T_{warm}	*GDD*
1	55	25	1.01	1	60	0.3	0.3	0.4	>5.0	>0.0	–	–	–
2	45	25	1	1	60	0.3	0.3	0.4	–	>0.0	–	–	–
3	40	25	1	1	25	0.3	0.3	0.4	–	>−5.0	<0.0	–	–
4	30	12.5	2	1	35	0.3	0.4	0.3	–	>−45.0	<0.0	–	>1100
5	40	25	1	1	35	0.3	0.3	0.4	–	>−45.0	<0.0	–	>1100
6	25	12.5	2.5	1	52	0.3	0.4	0.3	–	>−57.5	<−45.0	–	>350
7	30	25	1	1	52	0.3	0.3	0.4	–	>−57.5	<−45.0	–	>350
8	35	25	1	1	52	0.3	0.3	0.4	–	–	<−45.0	–	>350
9	27.5	12.5	1.5	1	5	0.45	0.4	0.15	–	–	–	–	>100
10	27.5	25	1	1	5	0.45	0.35	0.2	–	–	–	–	>100
11	15	20	1.25	1	–	0.45	0.55	0	–	–	–	>22.0	>100
12	25	20	1.5	1	–	0.45	0.55	0	–	–	–	–	>100

689 **Table 2** Comparison of observed and model-derived gross primary production (GPP; gC m^{-2} $month^{-1}$)
690 for 39 sites. The regression coefficients of slope (*a*), intercept (*b*), R^2, and root-mean-square error
691 (RMSE) are also shown. The PFT definitions are the same as in Table 1.

Longitude	**Latitude**	**Site**	**PFT**	**Years**	**GPP (gC m^{-2} $month^{-1}$)**			
					a	b	R^2	RMSE
131.15	-12.49	Au-How	2	2001-2006	1.54	-64.90	0.73	50.13
-68.75	45.21	US-Ho2	4	1999-2004	1.11	-2.42	0.97	18.95
-121.56	44.45	US-Me2	4	2002-2007	0.74	6.91	0.93	16.44
-121.61	44.32	US-Me3	4	2004-2005	1.14	14.96	0.91	18.20
-121.57	44.44	US-Me5	4	2000-2002	1.18	12.55	0.90	18.43
-76.67	35.80	US-NC2	4	2005-2006	0.64	62.28	0.85	25.13
-105.55	40.03	US-NR1	4	1998-2007	0.53	11.09	0.70	22.29
-89.87	34.25	US-Goo	5	2002-2006	0.54	128.53	0.48	53.27
-72.17	42.54	US-Ha1	5	1992-2006	0.65	67.39	0.69	59.59
-72.19	42.54	US-LPH	5	2002-2005	0.56	82.25	0.57	73.94
-86.41	39.32	US-MMS	5	1999-2006	0.67	89.27	0.70	53.94
-92.20	38.74	US-MOz	5	2004-2007	0.60	86.36	0.69	50.23
-82.24	29.76	US-SP2	5	1998-2004	0.27	160.04	0.25	36.50
-84.29	35.96	US-WBW	5	1995-1999	0.52	113.58	0.61	51.65
-98.48	55.88	CA-NS1	6	2002-2005	1.80	13.11	0.87	36.49
-98.52	55.91	CA-NS2	6	2001-2005	1.41	24.90	0.56	65.64
-98.38	55.91	CA-NS3	6	2001-2005	1.65	17.76	0.77	47.40
-98.38	55.91	CA-NS4	6	2002-2004	2.59	12.25	0.95	21.31
-98.49	55.86	CA-NS5	6	2001-2005	1.53	12.36	0.94	23.15
-99.95	56.64	CA-NS7	6	2002-2005	2.31	45.05	0.72	56.61
-121.95	45.82	US-Wrc	6	1998-2006	0.93	-7.75	0.81	34.30
-89.98	46.08	US-Los	7	2001-2005	0.74	98.07	0.52	75.02
-89.35	46.24	US-Syv	7	2001-2006	0.91	38.40	0.83	46.36
-90.08	45.81	US-WCr	7	1999-2006	0.78	54.64	0.75	59.25
-110.51	31.59	US-Aud	10	2002-2006	0.82	49.34	0.49	42.11
-155.75	68.49	US-Ivo	10	2003-2006	1.65	9.08	0.57	27.83
-80.67	28.61	US-KS2	10	2000-2006	0.45	148.76	0.36	25.63
-116.64	33.38	US-SO4	10	2004-2006	1.32	37.85	0.31	42.54
-120.95	38.41	US-Var	10	2001-2007	0.62	59.95	0.72	32.77
-98.04	35.55	US-ARb	12	2005-2006	0.27	103.38	0.34	45.75
-98.04	35.55	US-ARc	12	2005-2006	0.32	98.57	0.32	46.30
-97.49	36.61	US-ARM	12	2003-2006	0.80	106.17	0.28	57.43
-96.84	44.35	US-Bkg	12	2004-2006	1.05	62.24	0.59	69.07
-88.29	40.01	US-Bo1	12	1996-2007	0.33	123.55	0.26	88.55
-105.10	48.31	US-FPe	12	2000-2006	0.68	44.69	0.18	56.25
-93.09	44.71	US-Ro1	12	2004-2006	0.37	116.91	0.25	102.30
-93.09	44.72	US-Ro3	12	2004-2006	0.50	96.89	0.40	91.07
-109.94	31.74	US-Wkg	12	2004-2007	1.22	44.34	0.25	67.95
-96.86	37.52	US-Wlr	12	2001-2004	0.78	86.50	0.65	47.84

692

693 **Table 3** Comparison of model-derived forest carbon density (Mg C ha^{-1}) with those from other studies.
694 Pan et al. (2001) calculated carbon densities for both above- and below-ground biomass. Numbers in
695 brackets for Pan et al. (2011) show the AGB values assuming that the AGB accounts for 80% of total
696 biomass density.
697

Source	Method	Forest Carbon Density (Mg C ha^{-1})			Carbon Stock (Pg)
		Europe	North America	Global	Global
Goodale et al.(2002)	Forest Inventary	38.8	44.6		
Liski et al.(2003)	Forest Inventary	43	43		
Thurner et al.(2014)	Remote Sensing	60.8±22.4	45.3±17.1		
Pan et al.(2011)	Forest Inventary	60.5 (48.4)	68.7 (54.9)	94.2 (75.4)	362.6 (290.1)
This Study	Model	59.24±20.04	53.74±36.39	82.96	276.5

698 **Figure captions**

699 Fig. 1 Comparison of LAI for growing degree day (GDD) and growing season index
700 (GSI) phenology models for the site of (a) US-Ha1 and (b) US-WCr. MODIS 8-day LAI
701 values are also shown for comparison.

702

703 Fig. 2 Comparison of annual observed and modeled GPP (gC m^{-2} $year^{-1}$) for (a) baseline
704 run with default parameters from Kucharik et al. (2000) and (b) calibrated run with
705 parameters in Table 1. The dashed line shows the 1:1 line.

706

707 Fig. 3 Comparison of observed and modeled AGB (Mg ha^{-1}) for (a) baseline run with
708 default parameters from Kucharik et al. (2000) and (b) calibrated run with parameters in
709 Table 1. The dashed line shows the 1:1 line. Each point in the figure indicates the AGB
710 measured in one or more plots (average for more than one plot) within a $0.5° \times 0.5°$
711 model grid.

712

713 Fig. 4 (a) Modeled global patterns of AGB (Mg ha^{-1}) averaged for 2000–2010 and (b)
714 latitudinal AGB patterns.

715

716 Fig. 5 Spatial patterns of (a) estimated woody residence time (τ_w, years) based on
717 collected field data, (b) uncertainty of estimated $\tau_{w,}$ and (c) simulated AGB by estimated
718 τ_w for pan-tropic areas. The uncertainty is estimated as the standard deviation of the
719 resulting τ_w when 75% of the collected field plot data was randomly selected in each of

720 100 random forest simulation model runs. The estimated τ_w has a 1 km resolution and
721 was resampled to $0.5° \times 0.5°$ when used as parameters for IBIS simulations in this study.
722
723 Fig. 6 Comparison of observed and model simulated AGB by (a) default; (b) calibrated
724 and (c) estimated τ_w. Each point in the figure indicates the AGB measured in one or more
725 plots (average for more than one plot) within a $0.5° \times 0.5°$ model grid. Observed AGB
726 was mostly measured during 1990–2010 and the model simulations were the averaged
727 values during those corresponding years.
728
729 Fig. 7 Simulated temporal trends of AGB during 1759–2010 for different Plant Function
730 Types (PFTs) by IBIS. The green lines show the 500 test runs using the random τ_w data
731 ranging between the default and calibrated values; the red line shows the result of the
732 calibrated τ_w. All the test sites were randomly selected from Fluxnet; details of the sites
733 are provided in Table 1.
734
735 Fig.8 Difference between model-derived AGB driven by Princeton and CRU
736 meteorological forcing datasets. The Princeton and CRU forcing data are on daily and
737 monthly timescales, respectively.

738 **Figure 1**

739

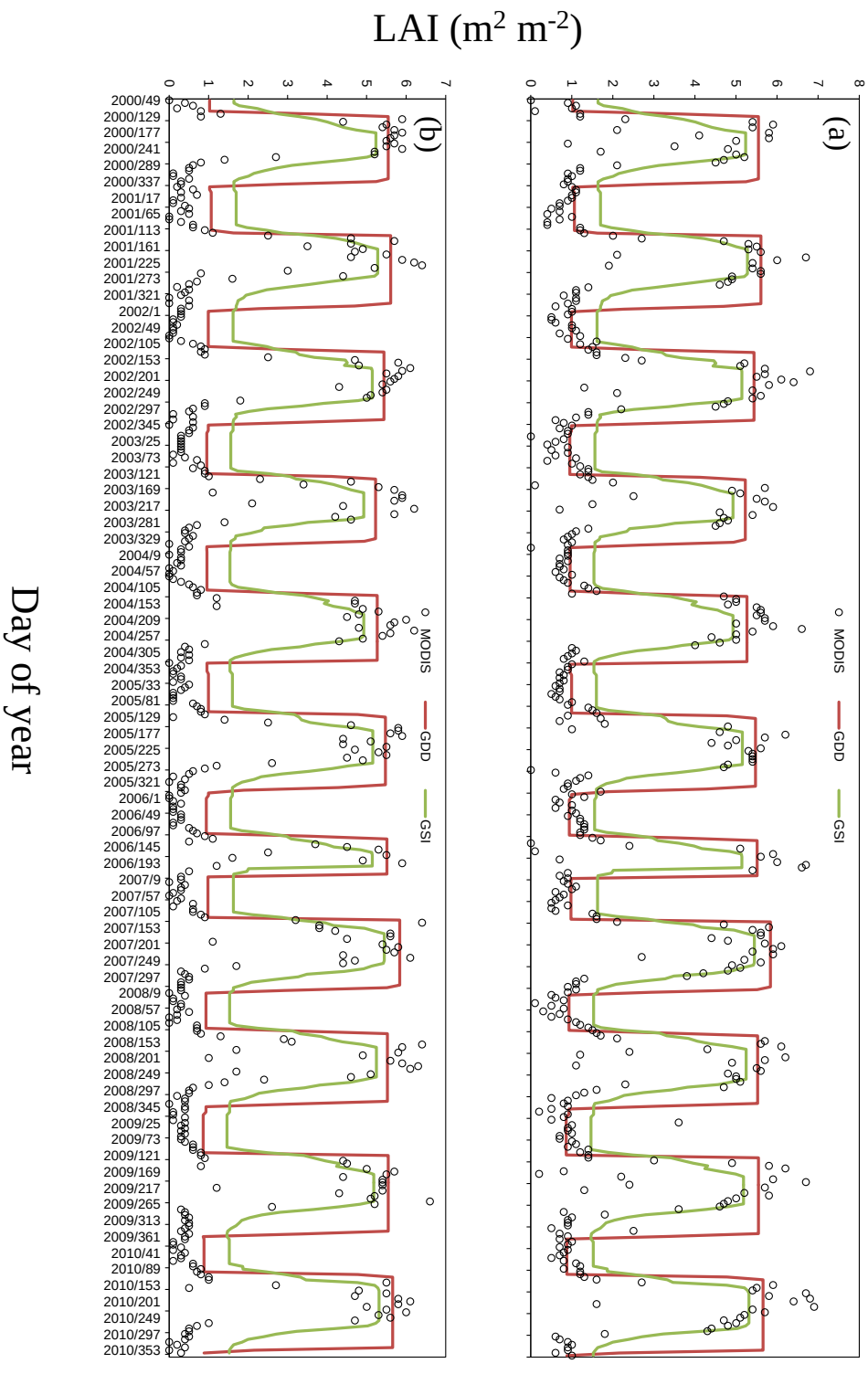

740

741 **Figure 2**

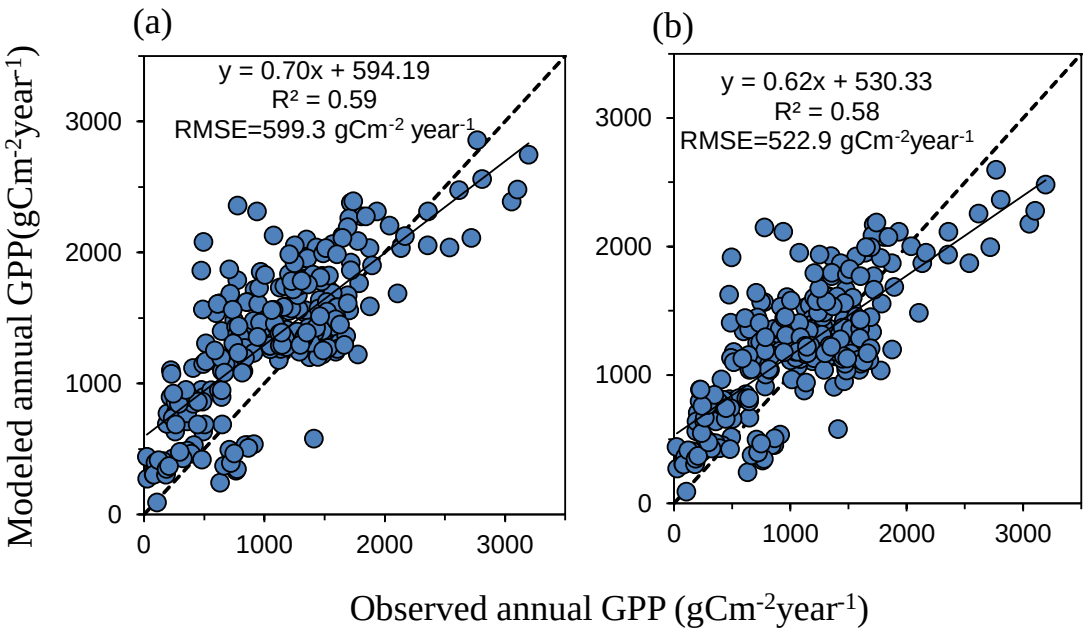

742

743 **Figure 3**

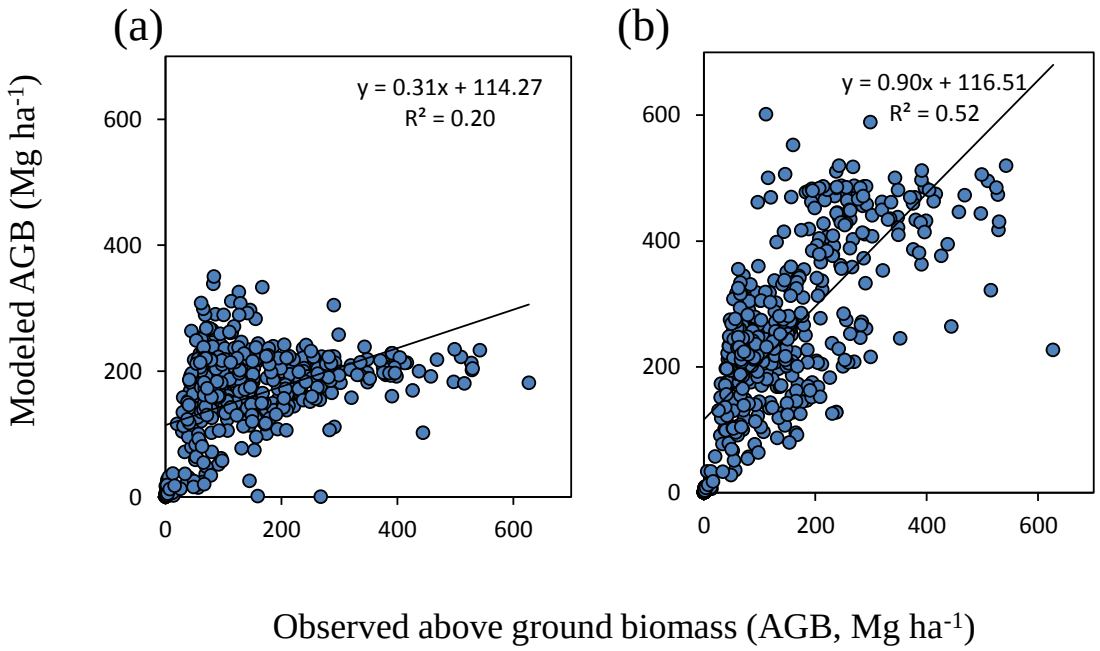

744

745 **Figure 4**

746

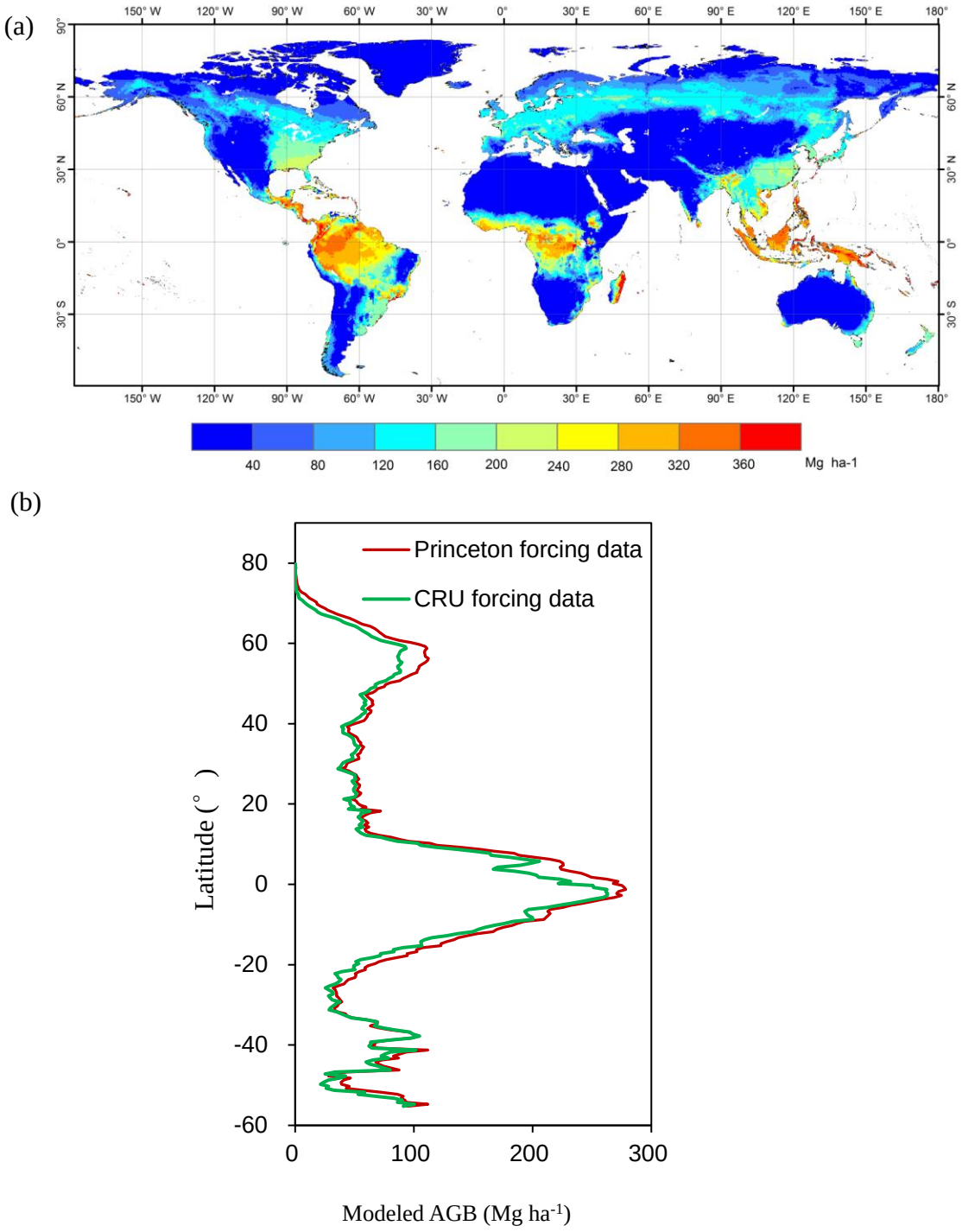

747

748 **Figure 5**

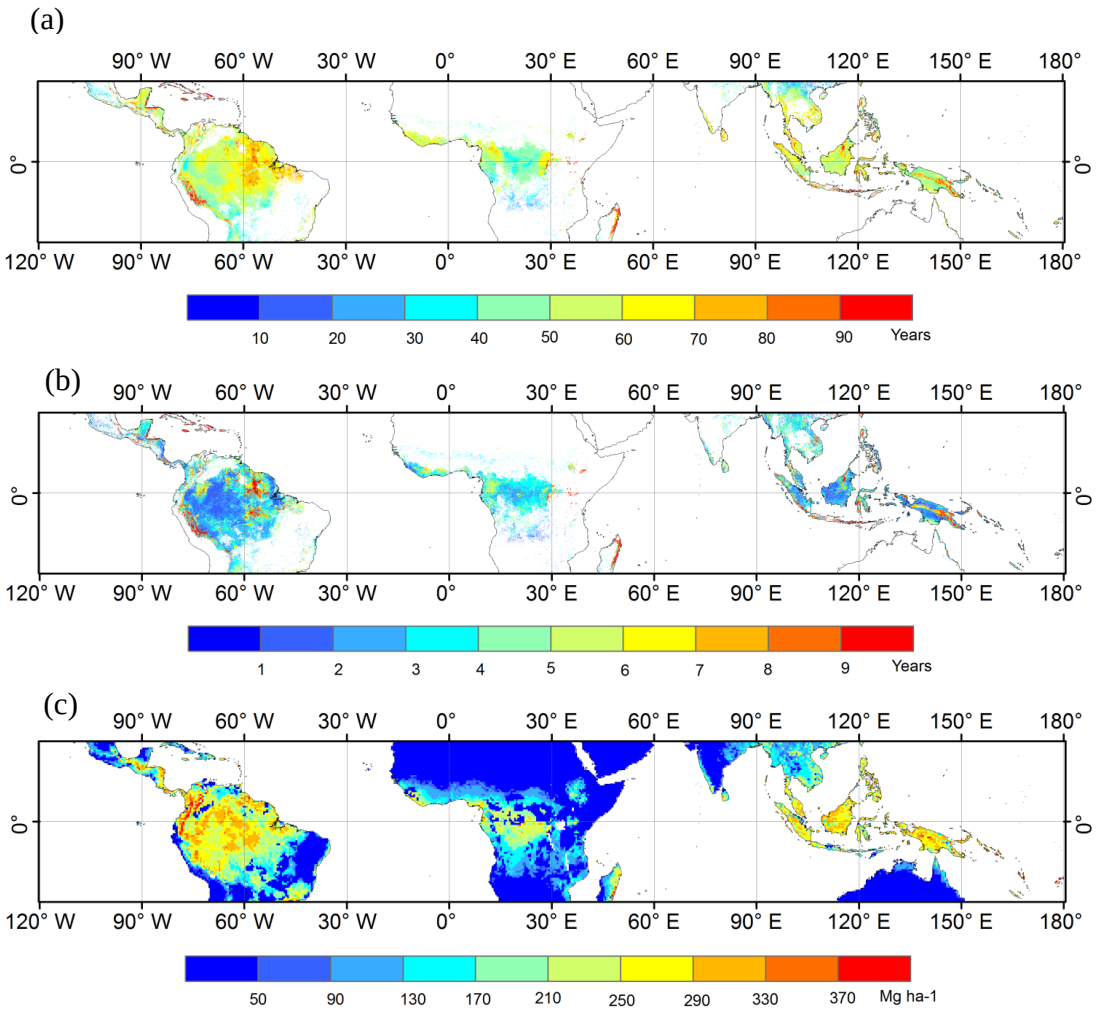

749

Figure 6

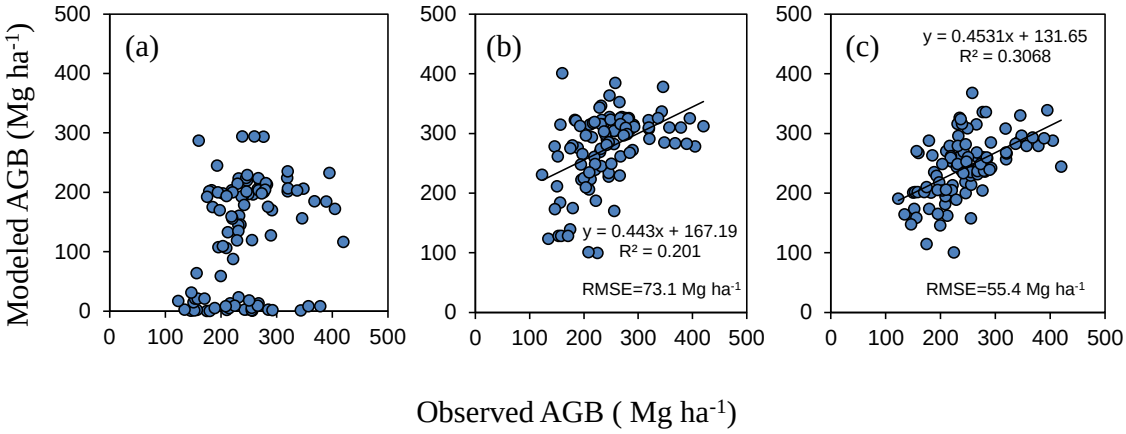
(a)
(b)
(c)
y = 0.443x + 167.19
R² = 0.201
RMSE=73.1 Mg ha-1
y = 0.4531x + 131.65
R² = 0.3068
RMSE=55.4 Mg ha-1
Modeled AGB (Mg ha-1)
Observed AGB (Mg ha-1)
0
100
200
300
400
500

752 **Figure 7**

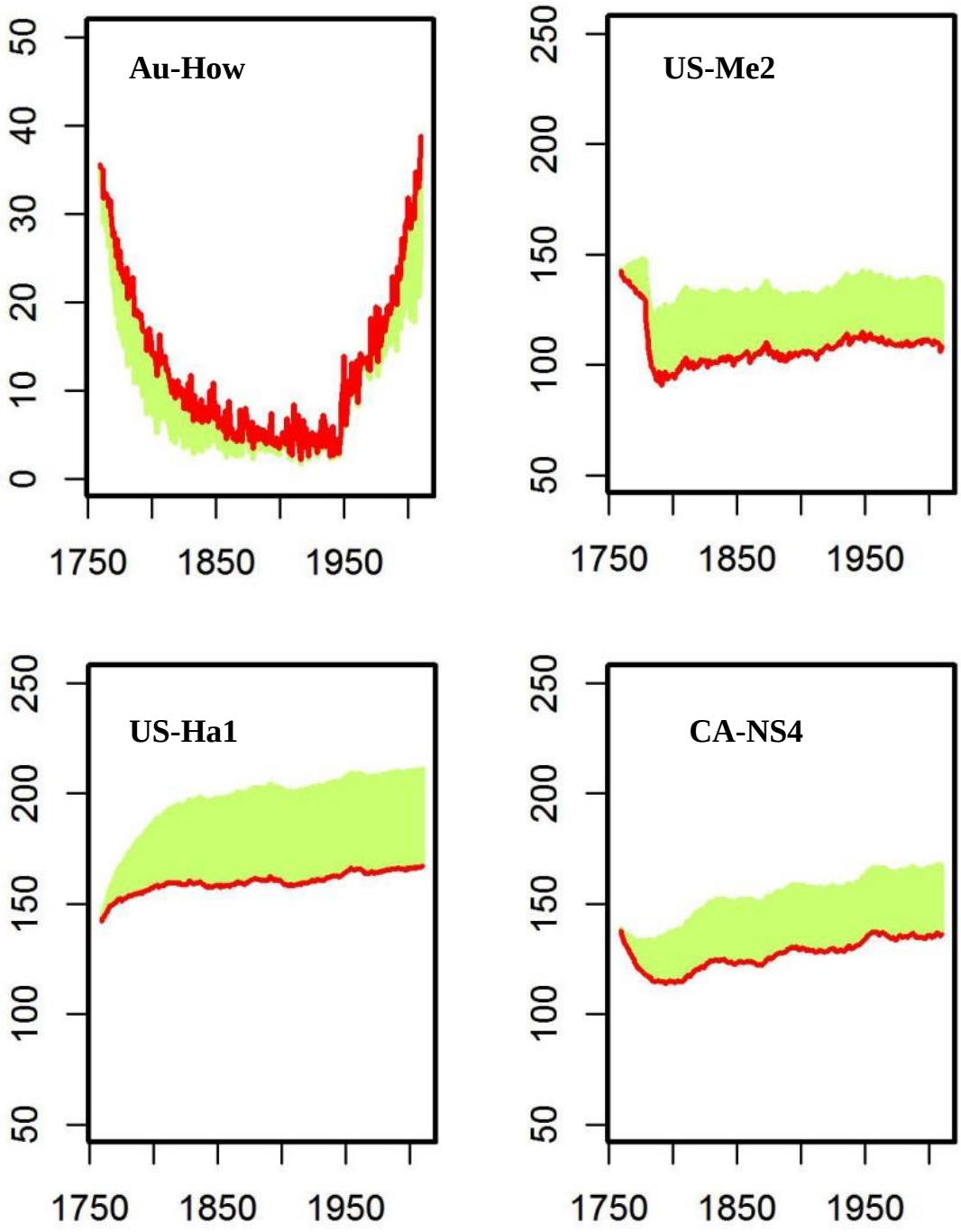

753

754 **Figure 8**

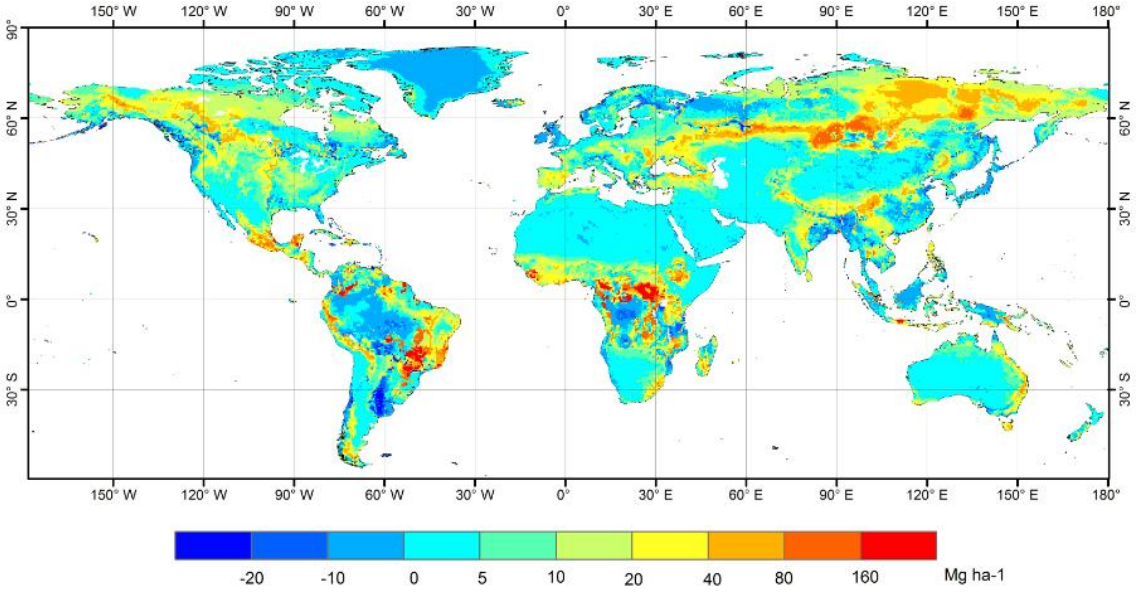

755

756